Inorg. Chem. **2005**, *44*, 6959–6966

Synthesis and X-ray Structure of the $Mn^{II}Cl_2$ and $Mn^{III}F_2$ Complexes of *N,N′*-Dimethyl-2,11-diaza[3,3](2,6)pyridinophane. High-Field Electron Paramagnetic Resonance and Density Funtional Theory Studies of the Mn(III) Complex. Evidence for a Low-Lying Spin Triplet State

Belén Albela,[†] Riccardo Carina,[†] Clotilde Policar,[‡] Sandrine Poussereau,[†] Joan Cano,[†,⊥] Jean Guilhem,[§] Luba Tchertanov,[§] Geneviève Blondin,[†] Michel Delroisse,[∥] and Jean-Jacques Girerd*,[†]

Laboratoire de Chimie Inorganique, UMR 8613, and Laboratoire de Chimie Bioorganique et Bioinorganique, UMR 8124, Institut de Chimie Moléculaire et des Matériaux d'Orsay, Université Paris-Sud, F-91405 Orsay, France, Laboratoire de Cristallochimie, Institut de Chimie des Substances Naturelles, UPR CNRS 2301, F-91198 Gif-sur-Yvette, France, Unilever Research Port Sunlight Laboratory, Wirral L63 3JW, U.K., and Departament de Química Inorgànica and Centre de Recerca en Química Teórica, Institució Catalana de Recerca i Estudis Avançats (ICREA), Universitat de Barcelona, Av. Diagonal 647, 08027 Spain

Received December 2, 2004

Two manganese complexes, $(py_2(NMe)_2)Mn^{II}Cl_2$ (**1**) and $[(py_2(NMe)_2)Mn^{III}F_2]^+$ (**2**), are here described with the macrocyclic ligand $py_2(NMe)_2$ ($py_2(NMe)_2$ = *N,N′*-dimethyl-2,11-diaza[3,3](2,6)pyridinophane). For both, the crystal structure is reported. The UV–visible spectrum of **2** exhibits a very broad near-infrared (NIR) band corresponding to the transition between the two e_g-type orbitals split by the Jahn–Teller effect. A negative *D* value of ca. -4 cm^{-1} was estimated by high-field and high-frequency electron paramagnetic resonance (HF-EPR) spectroscopy, which was consistent with symmetry considerations. Density functional theory (DFT) calculations on **2** support the $^5B_1$ electronic ground state predicted from the X-ray structure. Moreover, to explain the large value of the *D* parameter, a spin triplet first excited spin state was postulated to occur at low energy. This was confirmed by the DFT calculations.

Introduction

The macrocycle *N,N′*-dimethyl-2,11-diaza[3,3](2,6)pyridinophane[1,2] (noted here as $py_2(NMe)_2$) (see Scheme 1) is an interesting ligand that is able to wrap around a metal ion, while occupying four positions of an octahedron and leaving two *cis* positions free on which chemistry is possible. Koch and Kruger[3] have demonstrated that an Fe/$py_2(NMe)_2$ system catalyzes the degradative oxidation of catechols by O_2 in a dioxygenase-like reaction.

Scheme 1. $py_2(NMe)_2$ Ligand

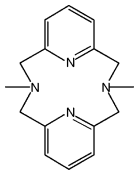

Here we report the synthesis and the structural characterization of two manganese derivatives, $(py_2(NMe)_2)Mn^{II}Cl_2$ (**1**) and $[(py_2(NMe)_2)Mn^{III}F_2](PF_6)$ (**2**(PF_6)), as well as a study of the electronic properties of the Mn(III) complex by density functional theory (DFT) calculations and high-field and high-frequency electron paramagnetic resonance (HF-EPR).[4]

* To whom correspondence should be addressed. E-mail: jjgirerd@icmo.u-psud.fr.
† Laboratoire de Chimie Inorganique, Université Paris-Sud.
‡ Laboratoire de Chimie Bioorganique et Bioinorganique, Université Paris-Sud.
§ Institut de Chimie des Substances Naturelles.
∥ Unilever Research Port Sunlight Laboratory.
⊥ Universitat de Barcelona.

(1) Bottino, F.; Di Grazia, M.; Finocchiaro, P.; Fronczek, F. R.; Mamo, A.; Pappalardo, S. *J. Org. Chem.* **1988**, *53*, 3521−3529.
(2) Alpha, B.; Anklam, E.; Deschenaux, R.; Lehn, J.-M.; Pietraskiewicz, M. *Helv. Chim. Acta* **1988**, *71*, 1042−1052.
(3) Koch, W. O.; Kruger, H.-J. *Angew. Chem., Int. Ed. Engl.* **1995**, *34*, 2671−2674.

10.1021/ic048302f CCC: $30.25
Published on Web 09/02/2005

Experimental Section

Preparation of Compounds. All chemical reagents were supplied by Aldrich and Acros and used without further purification. The ligand $py_2(NMe)_2$ was prepared according to the published procedure.[1]

$(py_2(NMe)_2)Mn^{II}Cl_2\cdot H_2O$ ($1\cdot H_2O$). $MnCl_2\cdot 6H_2O$ (186.6 mL of a 1 M solution in MeOH, 186.6 mmol) was added to $py_2(NMe)_2$ (0.05 g, 186.6 mmol) dissolved in 0.5 mL of CH_3CN. After 5 min yellow crystals formed (yield 80%). IR (KBr pellet): 3449, 2997, 2862, 2815, 1630, 1595, 1581, 1471, 1446, 1164, 1084, 1012, 875, 807, 796, 760, 444, 322 cm^{-1}. UV−vis (CH_3CN): λ_{max} (ϵ, M^{-1} cm^{-1}) = 375 (200) nm .

$[(py_2(NMe)_2)Mn^{III}F_2](PF_6)$ ($2(PF_6)$). MnF_3 (41.8 mg, 373 mmol) was dissolved in 5 mL of MeOH, and $py_2(NMe)_2$ (0.1 g, 373 mmol) in THF (5 mL) was added. After stirring for 30 min at room temperature, 4 mL of THF saturated in tetrabutylammonium hexafluorophosphate, NBu_4PF_6, was added. The resulting solution was left without stirring until the crystallization was finished. The product was collected by filtration (yield 80%). Anal. Calcd for $C_{16}H_{20}N_4MnF_8P$ (506.27 g mol^{-1}): C 38.35, H 3.75, N 11.32%. Found: C 37.94, H 3.95, N 11.1%. IR (KBr pellet): 3086, 2965, 2930, 2821, 1607, 1478, 1444, 1425, 1174, 1034, 1019, 844, 796, 603, 574, 555 cm^{-1}. UV−vis (CH_3CN): λ_{max} (ϵ, M^{-1} cm^{-1}) = 410 (42), 465 (95), 495 (110), 850 (25) nm.

Physical Measurements. Cyclic voltammetry was measured using an EGG PAR potentiostat (M 273 model). The working electrode was a Pt disk 3 mm in diameter, carefully polished with diamond pastes and ultrasonically rinsed in ethanol before use. A Pt wire was used as the counter electrode, and as the reference, a $Ag/AgClO_4$ electrode, prepared in acetonitrile and separated by a fritted disk from the main solution (calibration gave a potential of 530 mV vs normal hydrogen electrode (NHE)), was used. The experiment was carried out on a degassed solution by argon flushing. The ionic strength was kept constant by working in a 0.1 M NBu_4PF_6 solution in dry CH_3CN. Electronic spectra were recorded on a Varian Cary 5E spectrophotometer.

High-Field EPR Spectroscopy. Compound $2(PF_6)$ (25−30 mg) was thoroughly ground and dispersed in Nujol which was then frozen in liquid nitrogen. This was done to provide a random sampling and hinder crystallite orientation. A solution spectrum was also obtained by dissolving 20 mg in 200 μL of freshly distilled anhydrous dimethylformamide (DMF). Frequencies in the 284−296 GHz range were generated by a Gunn diode microwave source (Epsilon-Lambda Geneva) generating 100 mW of power over a 89−101 GHz frequency range and a frequency-tripler (Radiometric Physics, Meckenheim). The spectrometer has been described elsewhere.[5] Spectra were recorded in the 5−30 K temperature range. The simulations of the high-field EPR spectra were performed using XSophe software developed by the Centre for Magnetic Resonance and the Department of Mathematics at the University of Queensland, Brisbane, Australia, for Bruker Biospin GmbH.[6]

Table 1. Details of Structure Determination, Refinement, and Experimental Parameters for Compounds $1\cdot H_2O$ and $2(PF_6)$

	$1\cdot H_2O$	$2(PF_6)$
emperical formula	$C_{16}H_{20}N_4Cl_2Mn\cdot H_2O$	$C_{16}H_{20}N_4F_2MnPF_6$
formula weight (g mol^{-1})	411.21	506.27
temperature (K)	293	293
wavelength (Å)	0.71073	0.71073
crystal system	orthorhombic	monoclinic
space group	*Pbca*	$P2_1/c$
a (Å)	13.277(3)	9.402(5)
b (Å)	15.459(4)	15.825(8)
c (Å)	18.097(6)	13.343(5)
α (deg)	90	90
β (deg)	90	94.11(4)
γ (deg)	90	90
volume ($Å^3$)	3714(2)	1980.2(16)
Z	8	4
calculated density (g cm^{-3})	1.471	1.698
absorption coefficient (mm^{-1})	1.009	0.832
Θ range for data collection (deg)	4.7−62.8	4.0−60.0
index ranges	$0 < h < 18$	$-13 < h < 13$
	$0 < k < 21$	$0 < k < 22$
	$0 < l < 25$	$0 < l < 18$
reflections collected	5409	5989
independent reflections	5409 [R(int) = 0.0000]	5763 [R(int) = 0.0187]
data	2929	3878
R1 [$I > 2\sigma(I)$]	0.0636	0.0426
wR2	0.1704	0.1131
largest diff peak/hole (e^- $Å^{-3}$)	0.174/−0.545	0.606/−0.474

X-ray Crystallographic Data Collection and Refinement of the Structures. The crystal data and the parameters of data collection are summarized in Table 1. Prismatic crystals, light yellow (0.5 × 0.4 × 0.3 mm^3) of $1\cdot H_2O$ and transparent orange (0.5 × 0.25 × 0.15 mm^3) of $2(PF_6)$, were chosen for the X-ray diffraction experiments. The unit-cell and intensity data were measured with an Enraf-Nonius CAD-4 diffractometer with graphite monochromated Mo Kα radiation. The cell constants were obtained by least-squares procedures based upon the 2Θ values of 25 reflections measured in the ranges 20.8° < 2Θ < 21.4° for $1\cdot H_2O$ and 20.1° < 2Θ < 22.9° for $2(PF_6)$ at room temperature. Both structures were solved by direct methods with the program SHELXS86[7] and refined by using the SHELXL93[8] program. The drawings were prepared with ORTEPII.[9]

Both complexes were located in a general crystallographic position. The structures were refined anisotropically (non-hydrogen atoms) by a full-matrix least-squares approximation based on F^2. Hydrogen atom positions with the exception of water hydrogen in $1\cdot H_2O$ were calculated by assuming geometrical positions and were included in the structural model. Only one hydrogen atom of the water molecule in $1\cdot H_2O$ was found in a difference Fourier map and was isotropically refined. The second hydrogen atom could not be located and was, therefore, not included in the calculations. For both structures, an extinction correction was applied, but an empirical absorption correction[10] was made only for $1\cdot H_2O$. Crystallographic data (excluding structure factors) for the structures reported in this paper have been deposited at the Cambridge Crystallographic Data Centre as supplementary publication CCDC-103276 for $1\cdot H_2O$ and CCDC-103277 for $2(PF_6)$. Copies of the data can be obtained free of charge on application to CCDC,

(4) Abbreviations used in the text: **bipy**, 2,2′-bipyridine; **bpea**, *N*,*N*-bis(2-pyridylmethyl)ethylamine; **dbm**, 1,3-diphenyl-1,3-propanedione; **DFT**, density functional theory; **DMF**, dimethylformamide; **HF-EPR**, high-field and high-frequency electron paramagnetic resonance; **$LBzl_2$**, *N*,*N*′-bisbenzyl-*N*,*N*′-bis(2-pyridylmethyl)ethane-1,2-diamine; **LMCT**, ligand-to-metal charge transfer; **LUMO**, lowest unoccupied molecular orbital; **NHE**, normal hydrogen electrode; **NIR**, near-infrared; **$py_2(NMe)_2$**, *N*,*N*′-dimethyl-2,11-diaza[3,3](2,6)pyridinophane; **SOMO**, single occupied molecular orbital; **TD-DFT**, time-dependent density functional theory; **terpy**, 2,2′:6′,2″-terpyridine; **UV−vis**, ultraviolet−visible.

(5) Un, S.; Dorlet, P.; Rutherford, A. W. *Appl. Magn. Reson.* **2001**, *21*, 341−361.

(6) Griffin, M.; Muys, A.; Noble, C.; Wang, D.; Eldershaw, C.; Gates, K. E.; Burrage, K.; Hanson, G. R. *Mol. Phys. Rep.* **1999**, *26*, 60−84.

(7) Sheldrick, G. M. *SHELXS86, Program for the Solution of Crystal Structures*; University of Göttingen: Germany, 1986.

(8) Sheldrick, G. M. *SHELXL93, Program for the Refinement of Crystal Structures*; University of Göttingen: Germany, 1993.

(9) Johnson, C. K. *ORTEPII*; Report ORNL-5138; Oak Ridge National Laboratory: Oak Ridge, TN, 1976.

(10) Walker, N.; Stuart, D. *Acta Crystallogr., Sect. A* **1983**, *39*, 158.

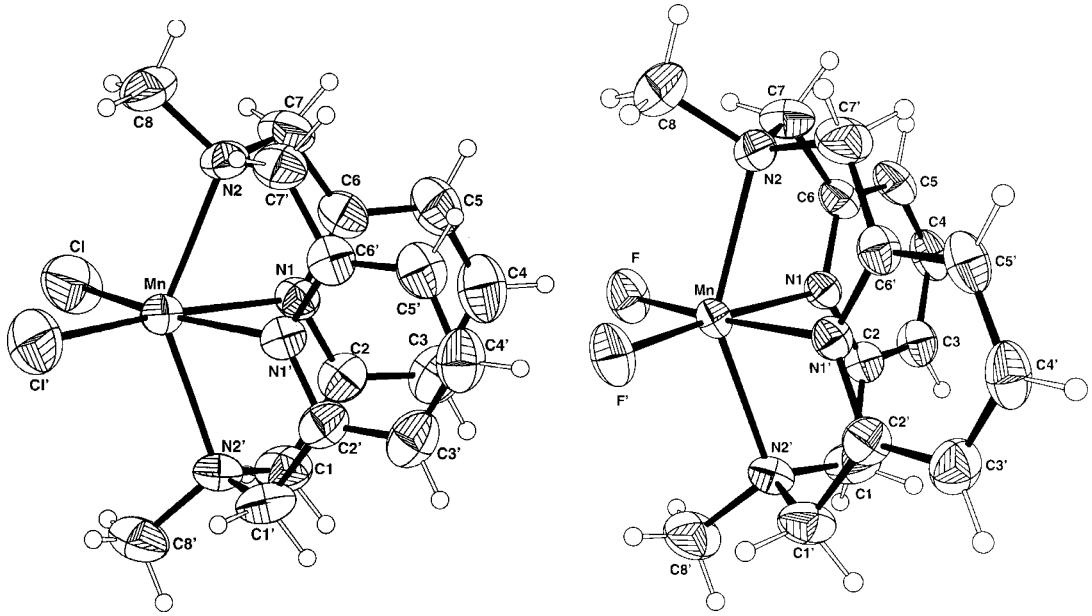

Figure 1. ORTEP diagrams of $(py_2(NMe)_2)MnCl_2$ **(1**, left) and the $[(py_2(NMe)_2)MnF_2]^+$ cation **(2**, right), showing the atomic numbering scheme. Displacement ellipsoids are drawn at the 50% probability level; H atoms are shown as small circles of arbitrary radii.

12 Union Road, Cambridge CB2 1EZ, U.K. Fax: +44 (1223)336-033. E-mail: deposit@ccdc.cam.ac.uk.

Computational Methodology. Density functional theory[11] was used to evaluate the electronic configuration of **2**(PF_6). The hybrid B3LYP method[12] has been used in the calculations as implemented in Gaussian98,[13] mixing the exact Hartree−Fock exchange with the Becke's expression for the exchange[14] and using the Lee−Yang−Parr correlation functional.[15] Basis sets of triple-ζ quality[16] (manganese atom) and of double-ζ quality[17] (atoms other than manganese) were used in all calculations. Excited-state energies and oscillator strengths were computed within the time-dependent density functional theory (TD-DFT) framework as implemented in the Gaussian98 program.[13]

Results and Discussion

Two mononuclear complexes were isolated using the $py_2(NMe)_2$ ligand. The first one is a hexacoordinated Mn(II) species with two coordinated chloride anions. It was obtained using $MnCl_2 \cdot 6H_2O$ as the source of manganese. The second one was synthesized using MnF_3 as the starting manganese salt. It is, thus, a Mn(III) system with two coordinated fluoride anions.

Table 2. Selected Bond Lengths (Å) and Angles (deg) in **1** and **2**

	1	**2**
Mn−N2	2.378(3)	2.274(2)
Mn−N2′	2.354(3)	2.278(2)
Mn−N1	2.247(3)	2.024(2)
Mn−N1′	2.266(3)	2.020(2)
Mn−Hal[a]	2.414(1)	1.801(2)
Mn−Hal′	2.403(1)	1.805(2)
N2−Mn−N2′	138.6(1)	147.03(8)
N2−Mn−N1	73.2(1)	77.07(8)
N2−Mn−N1′	73.4(1)	78.76(8)
N2−Mn−Hal	102.37(9)	98.40(8)
N2−Mn−Hal′	106.04(9)	105.31(8)
N2′−Mn−N1	73.9(1)	78.79(8)
N2′−Mn−N1′	73.7(1)	77.32(8)
N2′−Mn−Hal	101.5(1)	103.28(8)
N2′−Mn−Hal′	101.9(1)	97.40(8)
N1−Mn−N1′	73.5(1)	85.63(8)
N1−Mn−Hal	89.19(9)	88.95(8)
N1−Mn−Hal′	169.49(9)	175.27(8)
N1′−Mn−Hal	162.65(9)	174.33(7)
N1′−Mn−Hal′	96.2(1)	90.81(8)
Hal−Mn−Hal′	101.15(6)	94.69(8)

[a] Hal = Cl in **1**, and Hal = F in **2**.

X-ray Structures of $(py_2(NMe)_2)MnCl_2 \cdot H_2O$ $(1 \cdot H_2O)$ and $[(py_2(NMe)_2)MnF_2](PF_6)$ $(2(PF_6))$. A view of both the neutral Mn(II) complex $(py_2(NMe)_2)MnCl_2$ (**1**) and the monocationic Mn(III) complex $[(py_2(NMe)_2)MnF_2]^+$ (**2**) is presented in Figure 1. Selected bond lengths and angles are listed in Table 2. In both complexes, the manganese ion is coordinated by the four nitrogen atoms of the $py_2(NMe)_2$ ligand and by two halogen anions that are in *cis* positions one to the other. The two pyridine groups of the tetradentate ligand are in *trans* positions to the halogen anions. According to Table 2, the Mn ion in both complexes is in a distorted octahedral coordination sphere. The two halogen anions together with the two pyridine nitrogen atoms form, however, an equatorial plane that contains the metal center: the mean

(11) Parr, R. G.; Yang, W. *Density Functional Theory of Atoms and Molecules*; Oxford University Press: New York, 1989.
(12) Becke, A. D. *J. Chem. Phys.* **1993**, *98*, 5648−5652.
(13) Frisch, M. J.; Trucks, G. W.; Schlegel, H. B.; Scuseria, G. E.; Robb, M. A.; Cheeseman, J. R.; Zakrzewski, V. G.; Montgomery, J. A., Jr.; Stratmann, R. E.; Burant, J. C.; Dapprich, S.; Millam, J. M.; Daniels, A. D.; Kudin, K. N.; Strain, M. C.; Farkas, O.; Tomasi, J.; Barone, V.; Cossi, M.; Cammi, R.; Mennucci, B.; Pomelli, C.; Adamo, C.; Clifford, S.; Ochterski, J.; Petersson, G. A.; Ayala, P. Y.; Cui, Q.; Morokuma, K.; Malick, D. K.; Rabuck, A. D.; Raghavachari, K.; Foresman, J. B.; Cioslowski, J.; Ortiz, J. V.; Stefanov, B. B.; Liu, G.; Liashenko, A.; Piskorz, P.; Komaromi, I.; Gomperts, R.; Martin, R. L.; Fox, D. J.; Keith, T.; Al-Laham, M. A.; Peng, C. Y.; Nanayakkara, A.; Gonzalez, C.; Challacombe, M.; Gill, P. M. W.; Johnson, B.; Chen, W.; Wong, M. W.; Andres, J. L.; Gonzalez, C.; Head-Gordon, M.; Replogle, E. S.; Pople, J. A. *Gaussian 98*, Revision A.7; Gaussian Inc.: Pittsburgh, PA, 1998.
(14) Becke, A. D. *Phys. Rev. A* **1988**, *38*, 3098−3100.
(15) Lee, C.; Yang, W.; Parr, R. G. *Phys. Rev. B* **1988**, *37*, 785−789.
(16) Schäfer, A.; Huber, C.; Ahlrichs, R. *J. Chem. Phys.* **1994**, *100*, 5829−5835.
(17) Schäfer, A.; Horn, H.; Ahlrichs, R. *J. Chem. Phys.* **1992**, *97*, 2571−2577.

Scheme 2. Labeling of the Molecular Axes and of the C_{2v} Symmetry Elements

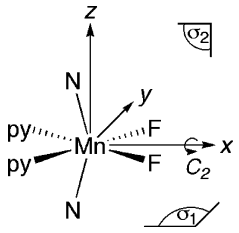

deviations from the least-squares plane formed by these five atoms are 0.014(2) Å in **1** and 0.035(1) Å in **2**, respectively. The two amine nitrogen atoms occupy the axial positions, with longer $Mn-N_{amine}$ distances than $Mn-N_{pyridine}$, whatever the oxidation state of the Mn ion. In **2**, this is characteristic of a Jahn−Teller elongation that develops toward the amine functions. The Mn−F and Mn−F′ bond lengths of 1.801(2) and 1.805(2) Å in cation **2** are shorter than the ones measured in [(bpea)$Mn(F)_3$], [(terpy)$Mn(F)_3$], where they are ranging from 1.8191(12) to 1.8511(6) Å,[18] or [(bipy)$Mn(F)_3(OH_2)$] (1.8386(14), 1.835(2), and 1.835(2) Å).[19] The metal−ligand bond lengths in **1** are, however, similar to those observed in the now numerous mononuclear Mn(II) complexes with a *cis*-N_4Cl_2 coordination sphere.[20]

Distortion from octahedral symmetry is also indicated by the bond angle values involving one axial ligand, the Mn ion, and one equatorial ligand or the second axial ligand that strongly differ from the ideal values of 90 or 180°, respectively. However, both units are close to the C_{2v} symmetry, with the C_2 axis bisecting the Hal−Mn−Hal′ angle. We will further refer to this symmetry group when labeling the d orbitals and the spectroscopic terms for complex **2** (see Scheme 2). Note that the macrocyclic ligand wraps in a "butterfly" form around the metal center that is different in **1** and **2**. While the two pyridine rings are nearly perpendicular in **2**, the dihedral angle decreases from 83.08(8)° in **2** to 42.7(2)° in **1**.

As mentioned previously, complex **1** crystallizes as the monohydrate. The water molecule is involved in two hydrogen bonds with the chloride ions of two different complexes with oxygen−chloride separations of 3.105(6) Å (O···Cl [x, y, z]) and 3.178(6) Å (O···Cl′ [$x + 0.5$, y, $-z + 0.5$]), respectively. A similar interaction was found in $[(LBzl_2)Fe^{II}Cl_2]\cdot H_2O$.[21]

The molecular arrangement in **2**(PF_6) shows another type of intermolecular interaction. The cations form infinite chains along the b axis held by $\pi-\pi$ interactions between the pyridine rings. Within the two pairs of involved aromatic cycles—one pair with primed numbered atoms, the other with unprimed numbered ones (see Figure S1 of the Supporting Information)—the pyridine fragments are almost exactly parallel, and their centroids are separated by 3.60 and 3.87 Å, respectively. An additional effect is the Mn−F···H−C intermolecular interactions. The geometrical characteristics are F···C4 3.287 Å, F···H4 2.496 Å, F···H4−C4 143.0°, F′···C4′ 3.347 Å, F′···H4′ 2.546 Å, and F′···H4′−C4′ 144.4°. These values provide evidence for the existence of good hydrogen bonds between the manganese−fluoride motif on one hand and the C−H extremity of one pyridine ring on the other.[22] As previously described by Brammer et al.,[22] the geometry is controlled by electronic effects. Indeed, the approach of the C−H fragment is more favored toward the p orbital of the halogen atom that is perpendicular to the M−F bond rather than toward the sp lone pair that runs on from the M−F bond. The later has a reduced charge density due to the involvement of one fluoride p orbital in the M−F σ-bond.

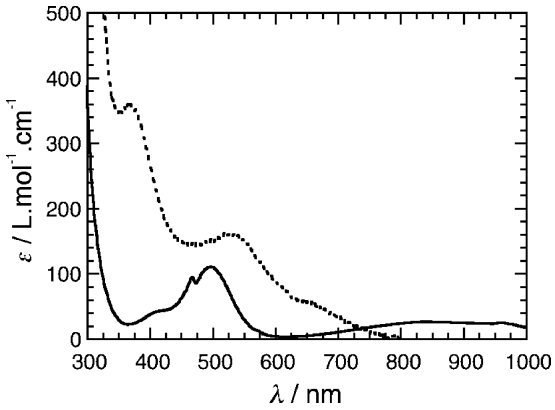

Figure 2. UV−visible spectra of an acetonitrile solution of **2** (solid line) and of the one electron oxidized form of **1** (dashed line).

UV−Visible Spectroscopy. The UV−visible spectrum of the orange acetonitrile solution of **2** is shown in Figure 2 (solid line). It presents bands of weak intensity at 410, 465, 495, and 850 nm, that is at 24390, 21500, 20200, and 11800 cm^{-1}, respectively. According to the low extinction coefficient values, they may be assigned to d−d transitions.[23, 24]

Assuming that complex **2** presents an elongation distortion that develops perpendicularly to the equatorial plane, the energetic diagram shown in Figure 3 can be drawn. The ground state results from an unoccupied d_{xy} orbital that points toward the equatorial ligands. Within C_{2v} symmetry, only three out of four d−d transitions are allowed. However, when lowering the symmetry down to C_s or C_2, the initially forbidden $^5B_1 \rightarrow {}^5B_2$ transition becomes allowed. Consequently, the 850 nm band is attributed to the $^5B_1 \rightarrow 1^5A_1$ transition, and the three bands detected in the 400−500 nm domain are attributed to transitions between the $^5B_1$ ground state and the $^5T_{2g}$ excited states. These assignments are

(18) Mantel, C.; Hassan, A. K.; Pécaut, J.; Deronzier, A.; Collomb, M.-N.; Duboc-Toia, C. *J. Am. Chem. Soc.* **2003**, *125*, 12337−12344.
(19) Núñez, P.; Elías, C.; Fuentes, J.; Solans, X.; Tressaud, A.; Marco de Lucas, M. C.; Rodríguez, F. *J. Chem. Soc., Dalton Trans.* **1997**, 4335−4340.
(20) Hureau, C.; Blondin, G.; Charlot, M.-F.; Philouze, C.; Nierlich, M. Cesario, M.; Anxolabéhère-Mallart, E. *Inorg. Chem.* **2005**, *44*, 3669−3683. See note 58 in this paper.
(21) Simaan, J.; Poussereau, S.; Blondin, G.; Girerd, J.-J.; Defaye, D.; Philouze, C.; Guilhem, J.; Tchertanov, L. *Inorg. Chim. Acta* **2000**, *299*, 221−230.
(22) Brammer, L.; Bruton, E. A.; Sherwood, P. *New J. Chem.* **1999**, *23*, 965−968.
(23) Dingle, R. *Acta Chem. Scand.* **1966**, *20*, 33−44.
(24) Davis, T. S.; Fackler, J. P.; Weeks, M. J. *Inorg. Chem.* **1968**, *7*, 1994−2002.

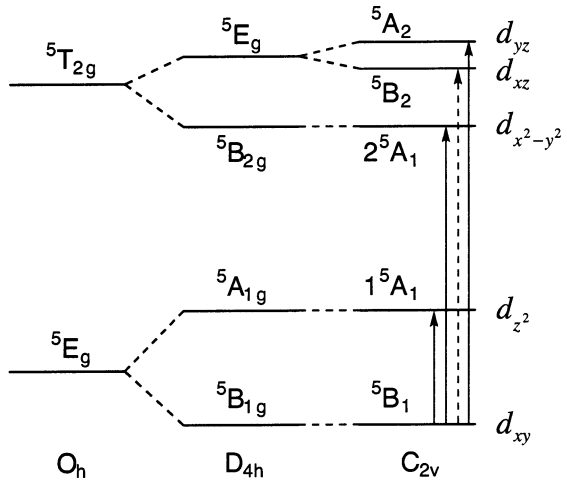

Figure 3. Splitting of the spectroscopic terms when lowering the symmetry from O_h to C_{2v} with the elongation axis perpendicular to the C_2 rotation axis. The labels refer to the symmetry elements shown in Scheme 2. The right column indicates the unoccupied d orbital. The solid and dashed arrows show the allowed and forbidden d−d transitions, respectively.

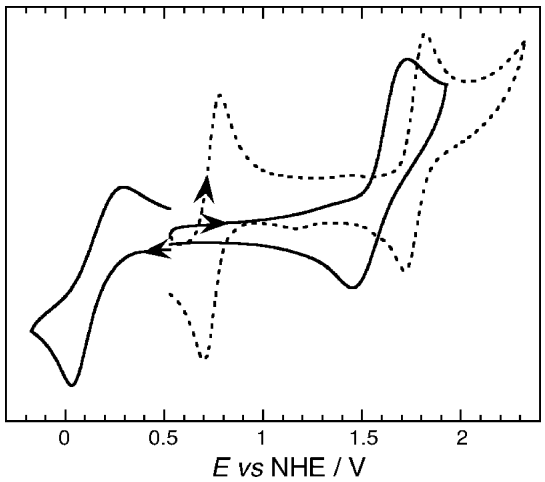

Figure 4. Cyclic voltammograms of complexes **1** (dashed line) and **2** (solid line) recorded at room temperature on acetonitrile solutions with 0.1 M NBu_4PF_6 as the supporting electrolyte (scan rate = 100 mV s^{-1}).

consistent with those published for $[MnF_6]^{3-}$ (ref 25) and $[(bipy)Mn(F)_3(OH_2)]$.[19]

The UV−visible spectrum of the violet acetonitrile solution of $[(py_2(NMe)_2)Mn^{III}Cl_2]^+$ (**1ox**) is presented in Figure 2 (dashed line). Bands at 370 and 530 nm are detected, with a shoulder at 650 nm. The 370 nm band is attributed to the $Cl^- \rightarrow$ Mn(III) ligand-to-metal charge transfer (LMCT) transition based on reported values for other Mn(III) complexes bearing a nitrogenous ligand.[23,26,27] The others are assigned to d−d transitions.

Cyclic Voltammetry. The electrochemistry of **1**·H_2O and **2**(PF_6) dissolved in acetonitrile with 0.1 M NBu_4PF_6 as a supporting electrolyte was investigated. All potentials were referenced in volts vs NHE.

Figure 4 shows the cyclic voltammograms of **1**·H_2O and **2**(PF_6) recorded at room temperature. In both cases, two quasi-reversible processes were observed at $E_{1/2} = 0.74$ V ($\Delta E_P = 0.08$ V) and $E_{1/2} = 1.77$ V ($\Delta E_P = 0.10$ V) for **1**·H_2O and at $E_{1/2} = 0.17$ V ($\Delta E_P = 0.27$ V) and $E_{1/2} = 1.59$ V ($\Delta E_P = 0.27$ V) for **2**(PF_6). These two features correspond to the redox couples Mn(II)/Mn(III) and Mn(III)/Mn(IV), respectively.

Fluoride is able to better stabilize higher oxidation states than chloride. It is interesting to see that the Mn(IV) ion is more oxidizing with chloride than with fluoride. This has already been shown by Armstrong et al. for Mn dimers.[28]

EPR Spectroscopy. A conventional EPR study (9 GHz) was performed for the Mn(II) complex, **1**, whereas HF-EPR was used for the Mn(III) compound, **2**(PF_6).

(A) 9 GHz EPR of 1. The EPR spectrum of a powder sample of **1**·H_2O shows a large isotropic resonance at $g =$ 2, which can be understood on the basis of an $S = {}^5/_2$ species presenting a small zero-field splitting effect. On frozen acetonitrile solution, a typical six-line hyperfine pattern is observed, with an average spacing of 9.1 mT (see Figure S2 of the Supporting Information).

(B) HF-EPR of 2(PF_6). High-spin Mn(III) (d^4, $S = 2$) is a non-Kramers ion. The EPR spectrum of such a Mn(III) ion can be adequately described by the spin Hamiltonian given by

$$H = D[S_z^2 - {}^1/_3S(S+1)] + E(S_x^2 - S_y^2) + \mu_B\mathbf{B}\cdot[g]\cdot\mathbf{S}$$

where D and E are the parameters describing the zero-field interaction, $[g]$ is the g matrix that characterizes the electronic Zeeman interaction, and **B** is the magnetic field vector. For the simplest case where the magnetic field and E are zero, the spin Hamiltonian describes five energy levels, two sets of which are doubly degenerate and are labeled $|\pm2\rangle$, $|\pm1\rangle$, and $|0\rangle$. The energy separation between these levels will be $3D$ and $1D$, respectively. If $D < 0$, $|\pm2\rangle$ will have lowest energy, while if $D > 0$, $|0\rangle$ will have the lowest. Application of a magnetic field will lift the degeneracies. In a low symmetry environment, a relatively large zero-field splitting ($|D| > 1$ cm^{-1}) is observed. This makes it difficult to retrieve reliable information from the conventional 9 GHz EPR spectrum of Mn(III) ions. Under certain circumstances, a broad feature corresponding to the $|-2\rangle \leftrightarrow |2\rangle$ transition can be observed using conventional frequencies.[29,30] In contrast, when the microwave excitation frequency is very high ($h\nu > |D|$), many other transitions can be observed and used to characterize the electronic structure of such integer-spin ions. This was first demonstrated in studies of Mn(III) porphyrin and corrole systems[31,32] and is now shown on a series of Mn(III) monomers.[18,33−38]

(25) Allen, G. C.; El-Sharkawy, G. A. M.; Warren, K. D. *Inorg. Chem.* **1971**, *10*, 2538−2546.
(26) Bellitto, C.; Tomlinson, A. A. G.; Furlani, C. *J. Chem. Soc. A* **1971**, 3267−3271.
(27) Triller, M. U.; Pursche, D.; Hsieh, W.-Y.; Pecoraro, V. L.; Rompel, A.; Krebs, B. *Inorg. Chem.* **2003**, *42*, 6274−6283.
(28) Pal, S. Olmstead, M. M.; Armstrong, W. H. *Inorg. Chem.* **1995**, *34*, 4708−4715.
(29) Dexheimer, S. L.; Gohdes, J. W.; Chan, M. K.; Hagen, K. S.; Armstrong, W. H.; Klein, M. P. *J. Am. Chem. Soc.* **1989**, *111*, 8923−8925.
(30) (a) Campbell, K. A.; Yikilmaz, E.; Grant, C. V.; Gregor, W.; Miller, A.-F.; Britt, R. D. *J. Am. Chem. Soc.* **1999**, *121*, 4714−4715. (b) Campbell, K. A.; Lashley, M. R.; Wyatt, J. K.; Nantz, M. H.; Britt, R. D. *J. Am. Chem. Soc.* **2001**, *123*, 5710−5719.

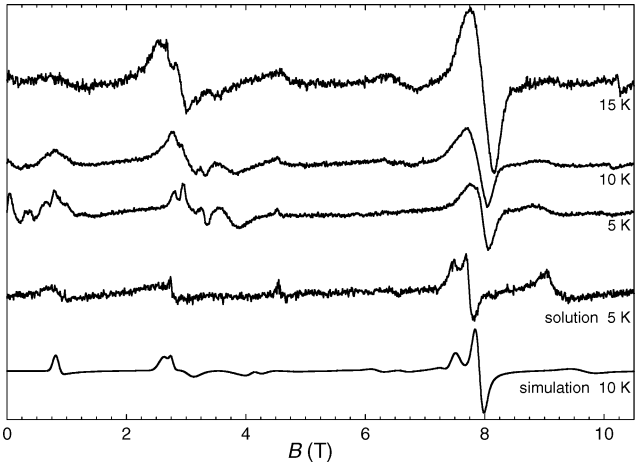

Figure 5. Powder high-field EPR spectrum of **2**(PF_6) at $T = 15$, 10, and 5 K (283.2 GHz) in the solid state and in solution (DMF) (285.5 GHz) at 5 K and a simulation for the 10 K spectrum (see text for details).

Figure 5 shows the EPR spectra of **2**(PF_6) using a 285 GHz excitation source obtained at 5, 10, and 15 K. They exhibit resonances in three regions: 0.5−1.0 T, 2.0−5.0 T, and 7.5−8.5 T. Signals arising from Mn(II) appeared above 10 T and are not shown. Although the exact line shapes of the resonances were sample dependent, the field positions were reproducible.

Symmetry considerations and DFT calculations (vide infra) predicted the sign of D to be negative. An estimate of the D amplitude was calculated by DFT. HF-EPR was used as an experimental support: the sign and estimate of D amplitude were obtained from HF-EPR at ca. 285 GHz. The sign of D was deduced directly from the temperature dependence of the feature at 1 T. This feature remained approximately constant between 5 and 10 K but rapidly decreased with increasing temperature. Preliminary simulations, performed within a closely axial symmetry, showed that D values in the neighborhood of -4 cm^{-1} allowed reproduction of the HF-EPR spectrum main features. The resonance at 1 T then arose from transition from either the $|+2\rangle$ or $|-2\rangle$ state.[39] Since the intensity of this resonance decreased with increasing temperature, this indicated that the $|\pm 2\rangle$ state was the lowest energy manifold. Hence, the temperature behavior was strongly indicative of a negative D value.

The lines for **2**(PF_6) were broader than those of the $Mn(dbm)_3$ monomer described by Barra et al.[33] To further examine this difference, we also recorded the spectrum of $Mn(dbm)_3$ under the same conditions as **2**(PF_6) and found the line width to be comparable to those originally published.[33] The Mn(III) ion in **2** is much less shielded by the ligands than in the case of $Mn(dbm)_3$, and the presence of extended chains within the crystallographic structure could promote intermolecular spin−spin interactions that would broaden EPR resonances. A solution spectrum of **2** in DMF (Figure 5) exhibits higher resolution of the main 8 T feature. This supported the contention that intermolecular interactions were at least one source of the line broadening. Further indications that crystal packing and spin−spin interactions had significant effects were the unexpected temperature-dependent resolution of various resonances and the appearance of a zero-field feature at 5 K, neither of which were apparent in the solution spectrum (Figure 5).

Anisotropy Effect in C_{2v}. With the exception of a diiodide complex,[35] it is well-known that, in a D_{4h} elongated geometry, the zero-field splitting tensor of a high-spin Mn(III) species is characterized by $D < 0$ and $E = 0$.[40] Within the C_{2v} symmetry where the two directions perpendicular to the elongation axis are differentiated, E can be different from zero. When only the quintet excited states are considered, it is indeed possible to show that the x, y, and z axes of Scheme 2 are the principal directions of the D tensor and of the g matrix (see the Supporting Information). Expressions of the principal values of the g matrix and of the D tensor are given below (see eqs 1a−e). The θ parameter ranges from 0 to 90° and indicates the mixing between the two $^5A_1$ states.

$$g_x = g_e - \frac{2\lambda}{E(^5B_2) - E(^5B_1)} \tag{1a}$$

$$g_y = g_e - \frac{2\lambda}{E(^5A_2) - E(^5B_1)} \tag{1b}$$

$$g_z = g_e - 8\lambda\left\{\frac{\sin^2\theta}{E(1^5A_1) - E(^5B_1)} + \frac{\cos^2\theta}{E(2^5A_1) - E(^5B_1)}\right\} \tag{1c}$$

$$D = \frac{\lambda}{2}\left\{g_z - \frac{g_x + g_y}{2}\right\} \tag{1d}$$

$$E = \frac{\lambda}{4}\{g_x - g_y\} \tag{1e}$$

These equations demonstrate that D is indeed negative. Using 80 cm^{-1} as an approximate value for the spin−orbit coupling constant λ,[41] using 20 000 cm^{-1} for the separation between the $^5B_1$ ground state and any of the $^5T_{2g}$ states, and

(31) (a) Goldberg, D. P.; Telser, J.; Krzystek, J.; Garrido Montalban, A.; Brunel, L.-C.; Barrett, A. G. M.; Hoffman, B. M. *J. Am. Chem. Soc.* **1997**, *119*, 8722−8723. (b) Krzystek, J.; Telser, J.; Pardi, L. A.; Goldberg, D. P.; Hoffman, B. M.; Brunel, L.-C. *Inorg. Chem.* **1999**, *38*, 6121−6129. (c) Krzystek, J.; Telser, J.; Hoffman, B. M.; Brunel, L.-C.; Licoccia, S. *J. Am. Chem. Soc.* **2001**, *123*, 7890−7897. (d) Bendix, J.; Gray, H. B.; Golubkov, G.; Gross, Z. *Chem. Commun.* **2000**, 1957−1958.
(32) Krzystek, J.; Telser, J. *J. Magn. Reson.* **2003**, *162*, 454−465.
(33) Barra, A.-L.; Gatteschi, D.; Sessoli, R.; Abbati, G. L.; Cornia, A.; Fabretti, A. C.; Uytterhoeven, M. G. *Angew. Chem., Int. Ed. Engl.* **1997**, *36*, 2329−2331.
(34) Limburg, J.; Vrettos, J. S.; Crabtree, R. H.; Brudvig, G. W.; de Paula, J. C.; Hassan, A.; Barra, A.-L.; Duboc-Toia, C.; Collomb, M.-N. *Inorg. Chem.* **2001**, *40*, 1698−1703.
(35) Mossin, S.; Weihe, H.; Barra, A.-L. *J. Am. Chem. Soc.* **2002**, *124*, 8764−8765.
(36) Krzystek, J.; Yeagle, G. J.; Park, J.-H.; Britt, R. D.; Meisel, M. W., Brunel, L.-C.; Tesler, J. *Inorg. Chem.* **2003**, *42*, 4610−4618.
(37) Tregenna-Piggott, P. L. W.; Weihe, H.; Barra, A.-L. *Inorg. Chem.* **2003**, *42*, 8504−8508.
(38) Aromí, G.; Telser, J.; Ozarowski, A.; Brunel, J.-C.; Stoeckli-Evans, H.-M.; Krzystek, J. *Inorg. Chem.* **2005**, *44*, 187−196.
(39) To provide accurate values for D, E, and (g_x, g_y, g_z), a multifrequency simulation is necessary. This was not the purpose of the present study.
(40) Gerritsen, H. J.; Sabisky, E. S. *Phys. Rev.* **1963**, *132*, 1507−1512.
(41) For instance, Gerritsen and Sabisky[40] use $\lambda = 60$ cm^{-1}, taking into account covalency reduction, and Barra et al.[33] use the free ion value $\lambda = 90$ cm^{-1}. For this qualitative discussion, we use an intermediate value.

assuming that the 2^5A_1 state corresponds to a hole in the $d_{x^2-y^2}$ orbital ($\theta = 0$), one obtains $D = -0.96$ cm^{-1}. Its absolute value is indeed much smaller than the one measured experimentally. Increasing the θ mixing coefficient decreases D. However, -1.85 cm^{-1} is the lowest value calculated when the hole in the $d_{x^2-y^2}$ orbital corresponds to the 1^5A_1 state that lies 11 800 cm^{-1} above the $^5B_1$ state. The absolute value of the D parameter is still smaller than the experimentally obtained value, 4 cm^{-1}.

It has been very convincingly shown by several authors[31b,33,40] that excited triplet states must be included in the calculation of D. As an analogy to what is found in D_{4h} or C_{4v} symmetry,[31b,33] the relevant triplet states are those associated with the electronic configurations $(d_{xy})^1(d_{xz})^1(d_{yz})^2$ and $(d_{xy})^1(d_{xz})^2(d_{yz})^1$ (^{3}E). The principal directions of the D tensor are not modified, and eq 2 gives the expression of the D' correction to the D parameter.[31b]

$$D' = -\frac{4\lambda^2}{E(^3\mathrm{E}) - E(^5\mathrm{B}_1)} \qquad (2)$$

One can, thus, evaluate the fact that the triplet state will lie 8400−11 900 cm^{-1} above the $^5B_1$ ground state. This crude estimate suggests that the first excited state in this type of mononuclear Mn(III) complex could well be a spin triplet. Indeed, an inspection of the Tanabe−Sugano diagram for d^4, taking $Dq = 2000$ cm^{-1} and $B = 800$ cm^{-1} (see ref 42), shows that $^3T_1$ would be only 1200 cm^{-1} above the ^{5}E ground state. DFT calculations shown below confirm that the first excited state is indeed a triplet state.

The zero-field splitting E value is evidently directly related to the splitting of the ^5E_g state into its $^5A_2$ and $^5B_2$ components. Its calculation is difficult since we do not know with precision the energy separations between these states and the ground $^5B_1$ level.

Assuming a zero mixing coefficient for the $^5A_1$ states ($\theta = 0$), $\lambda = 80$ cm^{-1}, and that the $^5T_{2g}$ states lie 20 000 cm^{-1} above the ground $^5B_1$ state, one finds $g_z = 1.970$ and $g_x = g_y = 1.994$.

Theoretical Calculations. The electronic structure of **2** was also investigated using DFT and TD-DFT methods.[43−45] The calculated electronic structure in the quintet ground state is shown in Figure 6. Three t_{2g} orbitals and one e_g orbital make up the set of *single occupied molecular orbitals* (SOMOs). Due to the C_{2v} symmetry of this complex, a full split of the t_{2g} orbitals was obtained. The highest energy SOMO was mainly composed of the d_{z^2} orbital of the manganese ion, whereas the *lowest unoccupied molecular orbital* (LUMO) possessed a manganese d_{xy} character. This confirmed that the d_{z^2} orbital was lower in energy than the d_{xy} orbital so that the ground state, within a supposed C_{2v} symmetry, was indeed the $^5B_1$ one and the system was close to axiality, which confirmed that θ was close to 0. Moreover, the calculation showed that the d_{xz}, $d_{x^2-y^2}$, and d_{yz} orbitals were very close in energy to each other (Figure 6). Because of the low symmetry of complex **2**, four nonforbidden transitions at different energies could be observed. The calculated UV−vis spectrum is shown in Figure 7. In this figure, we find four transitions of weak intensity corresponding to the d−d transitions in the manganese(III) ion. The calculated bands were at 801, 459, 447, and 405 nm (Table 3). In general, a good agreement was found with the experimental data. However, there were small differences

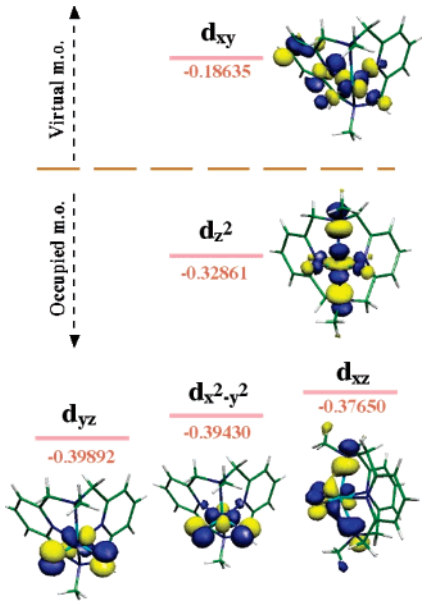

Figure 6. d-rich MOs of $[(py_2(NMe)_2)MnF_2]^+$ (**2**) as obtained by DFT calculation on the $^5B_1$ ground state.

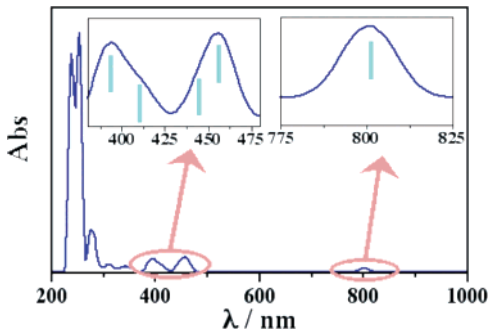

Figure 7. Calculated UV−vis spectrum of $[(py_2(NMe)_2)MnF_2]^+$ (**2**) as obtained by TD-DFT calculation.

Table 3. Characteristics of the Calculated UV−Visible Transitions for Complex **2**

transition[a]	λ (nm)	energy (cm^{-1})	f[b]	type	nature[c]	states
1	801	12 485	2.6×10^{-4}	d−d	$d_{z^2} \rightarrow d_{xy}$	$^5B_1 \rightarrow 1^5A_1$
2	459	21 785	9.4×10^{-4}	d−d	$d_{x^2-y^2} \rightarrow d_{xy}$	$^5B_1 \rightarrow 2^5A_1$
3	447	22 370	5.6×10^{-5}	d−d	$d_{xz} \rightarrow d_{xy}$	$^5B_1 \rightarrow {}^5B_2$
4	405	24 690	6.6×10^{-5}	d−d	$d_{yz} \rightarrow d_{xy}$	$^5B_1 \rightarrow {}^5A_2$
5	392	25 510	7.7×10^{-4}	CT[d]		

[a] Transition labels are shown in Figure 7. [b] The symbol f stands for the oscillator strength. [c] The d−d transitions are indicated according to the electron motion. [d] Charge-transfer band.

(42) Lever, A. B. P. In *Inorganic Electronic Spectroscopy*; Lappert, M. F., Ed.; Physical Inorganic Chemistry, Monograph 1; Elsevier: Amsterdam, The Netherlands, 1968.
(43) Runge, E.; Gross, E. K. U. *Phys. Rev. Lett.* **1984**, *52*, 997−1000.
(44) Gros, E. K. U.; Dobson, J. F.; Petersilka, M. In *Density Functional Theory*; Nalewajski, R. F., Ed.; Springer Series Topics in Current Chemistry Vol. 181; Springer: Berlin, 1996.
(45) Petersilka, M.; Gossmann, U. J.; Gross, E. K. U. *Phys. Rev. Lett.* **1996**, *76*, 1212−1215.

between the experimental and calculated energy values for the excited states. These differences could be due to (i) a small structural change in the complex in solution and (ii) the well-known effects of the solvent. The lower energy excitation corresponds to the transition $d_{z^2} \rightarrow d_{xy}$ ($^5B_1 \rightarrow 1^5A_1$). The assignment of the rest of the transitions ($t_{2g} \rightarrow e_g$) was facilitated by the results of the calculations. So, the experimentally observed bands at 495, 465, and 410 nm were assigned to the transitions $d_{x^2-y^2} \rightarrow d_{xy}$, $d_{xz} \rightarrow d_{xy}$, and $d_{yz} \rightarrow d_{xy}$ ($^5B_1 \rightarrow 2^5A_1$, $^5B_1 \rightarrow {}^5B_2$, and $^5B_1 \rightarrow {}^5A_2$), respectively (Table 3). From the calculations, we observed that small contributions of the metal−ligand (Mn−p orbital of L, transition 5 and others in Table 3) and ligand−metal (F−Mn, at lower energies) charge-transfer transitions hid some of the very weak d−d transitions. However, the calculations allow us to distinguish between these two kinds of transitions and to identify the nominally forbidden transitions. So, the $^5B_1 \rightarrow {}^5B_2$ forbidden transition was predicted to have a molar extinction coefficient 15 times lower than that of the $^5B_1 \rightarrow 2^5A_1$ transition, considering the same half-width at half-height coefficient for the two bands.

As previously mentioned, considering the quintet excited spin states obtained by d−d excitations is not sufficient to reproduce the large value of the zero-field splitting parameter *D*. To make sense of this *D* value, a DFT calculation of the energy of the lowest triplet state, using the experimental structural parameters, led to an excitation energy of 7210 cm^{-1}. So, the lower excited state is a triplet state that corresponds to removing the α electron of the d_{z^2} orbital and to putting a β electron in a mixture of the d_{xz} and d_{yz} orbitals. This triplet state indeed corresponds to what is expected from the theory of porphyrin complexes.[31b]

The transition from the ground state to the triplet excited state is difficult to detect in the UV−vis spectrum due to its low intensity, since it is a spin-forbidden excitation. The introduction of the triplet excited state in the evaluation of the *D* parameter allowed us to obtain a value that was on the order of the experimental one. So, assuming $\theta = 0$ and $\lambda = 80$ cm^{-1}, a *D* value of -4.45 cm^{-1} is deduced, in good agreement with the one found by EPR measurements. This λ value is slightly lower than the one corresponding to the free ion. The λ value needed to obtain a *D* value equal to the experimental one is $\lambda = 76$ cm^{-1}, which corresponds to an orbital reduction factor $\kappa = 0.84$. This value is just at the lower limit of the expected values for the usual ligand field.[42]

The real energy for the triplet excited state is likely to be smaller than the calculated one because the geometry relaxation in the triplet and quintet spin states is different. However, due to the occupation of an antibonding e_g orbital which points to the bonding directions, the quintet state shows in its relaxed geometry a bigger volume than the triplet state does. So, the quintet state will suffer a stronger lattice pressure in the solid state. Furthermore, this state, when in solution, will have a more energetic relaxation than the triplet state and, consequently, the energetic gap between these states will be larger. In this way, bigger values for λ allowed us to reproduce the same values for the *D* parameter.

Conclusion

Two Mn complexes, $(py_2(NMe)_2)Mn^{II}Cl_2 \cdot H_2O$ (**1**·H_2O) and $[(py_2(NMe)_2)Mn^{III}F_2](PF_6)$ (**2**(PF_6)), were synthesized with the quadridentate macrocycle ligand $py_2(NMe)_2$. X-ray analysis gave the detailed geometry of those two complexes. A remarkable feature was the large Jahn−Teller distortion observed for **2**. Three oxidation states, Mn(II), Mn(III), and Mn(IV), can be observed by cyclovoltammetry. The ligand stabilizes Mn(III), and fluoride supports this stability even more than the chloride anion. Using high-field EPR spectroscopy, it was possible to detect resonances for **2** and to evaluate the zero-field splitting parameters. The negative sign found for *D* was in agreement with the elongated Jahn−Teller distorted structure identified by X-ray diffraction. This result was confirmed by DFT calculations. A low-lying spin triplet state was necessary to explain the observed *D* value, and the excitation energy corresponding to this triplet state was calculated by DFT. The implications of such a low-lying spin state on the electronic properties of coupled Mn clusters will be explored.

Acknowledgment. This work has been supported in part by a grant from Unilever Company. R.C. gratefully acknowledges the Unilever Company for a postdoctoral position. We wish to acknowledge the Département de Biologie Joilot-Curie of CEA-Saclay and Sun Un for the use of the high-field EPR facility and initial involvement in the project.

Supporting Information Available: Arrangement of complex **2** as linear chains, shown in Figure S1. 9 GHz EPR spectrum recorded on a frozen acetonitrile solution of **1**, presented in Figure S2. Expressions within C_{2v} symmetry of the *g* matrix and of the zero-field splitting tensor. This material is available free of charge via the Internet at http://pubs.acs.org.

IC048302F